Journal of Materials Chemistry A

Accepted Manuscript

ROYAL SOCIETY OF CHEMISTRY

www.rsc.org/materialsA

Journal of
Materials Chemistry A

Dynamic Article Links ►

Cite this: DOI: 10.1039/c0xx00000x

www.rsc.org/xxxxxx

Full paper

Synergistic Integration of Thermocatalysis and Photocatalysis on Black Defective $(BiO)_2CO_3$ Microspheres

Fan Dong [a,*], Ting Xiong [a], Yanjuan Sun [a], Hongwei Huang [b], and Zhongbiao Wu [c,*]

Abstract: A novel environmental catalyst, black defective $(BiO)_2CO_3$ microspheres, was prepared by a vacuum heat treating method. It was interesting to discover that the as-obtained catalyst contained Bi element phase, Bi^{5+} ions and oxygen defects. These components endowed the black $(BiO)_2CO_3$ microspheres with efficient catalytic performance in NO removal. In situ DRIFTS investigation demonstrated that the adsorbed NO molecules at active sites (Bi^0, Bi^{5+} and oxygen defects) could react with the O_2 activated by oxygen defects to produce nitrogen dioxide, nitrite and nitrate in the dark. When the visible light was applied, highly enhanced catalytic activity can be achieved. On one hand, the visible light was transformed to thermal energy, accelerating the thermocatalytic reaction. On the other hand, the visible light could directly initiate the photocatalysis reaction as the generated oxygen defects could narrow the band gap of $(BiO)_2CO_3$, and the plasmonic effect of Bi element promoted the separation of electron-hole pairs. The highly efficient performance for NO removal under visible irradiation was correlated with the synergistic integration of thermocatalysis and photocatalysis. In addition, a facile method was developed to activate and regenerate the used catalyst for recycled application. This work could provide an innovative technology for NO removal by exploiting the synergistic integration of room temperature catalysis and visible photocatalysis and open up new opportunities in the design of efficient and low-cost catalysts for air purification.

1. Introduction

Recently, air quality has surged to worldwide attention due to the increasing awareness of the public environment and health. NOx (NO and NO_2), SO_2 and volatile organic compounds are often found in buildings, houses, cars and polluted urban atmospheres.[1] Of these pollutants, excess NOx mainly emitted from the combustion of fossil fuels could lead to serious environmental and health problems including acid rain, photochemical smog, and even pulmonary edema.[2,3] To date, various technologies such as physical adsorption, biofiltration, selective catalytic reduction, thermal catalysis and photocatalysis have been developed to remove NOx in air.[4-8]

Among the available technologies for the removal of air pollutants, thermal catalysts such as metal/oxides (Pt/Fe_2O_3, Au/CeO_2, and Au/TiO_2) and transition metal oxides (Ce–Mn, MnOx) have been extensively studied.[9-13] In these catalytic reactions, O_2 activation is the key step. Defects, especially oxygen vacancies, are the most reactive sites on the catalysts surface. Besenbacher et al. provided the evidence that the diffusion rate of the adsorbed molecular O_2 was dependent on the surface oxygen vacancy density with time-resolved scanning

[a] Chongqing Key Laboratory of Catalysis and Functional Organic Molecules, College of Environment and Resources, Chongqing Technology and Business University, Chongqing, 400067, China.
[b] Beijing Key Laboratory of Nonmetallic Minerals and Material Utilization of Solid Wastes, China University of Geosciences, Beijing 100083, China.
[c] Department of Environmental Engineering, Zhejiang University, Hangzhou 310027, China.
*To whom correspondence should be addressed.
E-mail: dfctbu@126.com (Fan Dong), zbwu@zju.edu.cn (Zhongbiao Wu).
Tel.: +86-23-62769785-605; Fax: +86-23-62769785-605.
Electronic supplementary information (ESI) available: Detailed and additional figures as noted in the text. See DOI: 10.1039/b000000x

tunneling microscopy.[14] The surface oxygen vacancies act as abundant surface donors for trapping electrons and function as adsorption sites for simple molecules. When excess electrons are present, molecular O_2 located at the oxygen defects sites are adsorbed in either superoxo (O_2^-), peroxo (O_2^{2-}), or dissociated ($2 \times O^{2-}$) form.[15-17] Importantly, these anions are active species, which can subsequently initiate chemical reaction for air pollutants removal.[11,18] Besides thermocatalysis, oxygen defects are found to play crucial roles in photocatalysis as well.

Photocatalysis offers great potential opportunities to tackle the environmental contamination and energy crisis problems by utilizing free and renewable sunlight. Photocatalysts including metal-containing semiconductors, metal-free semiconductors and plasmonic metals have been successfully applied in environmental remediation.[19-24] As most of semiconductor photocatalysts possess large band gaps and could only work under UV light irradiation, a large variety of approaches have been developed to extend the light absorption spectra, involving doping, metal loading and compositing.[25-28] Notably, introduction of oxygen defects in oxide semiconductor is supposed to be conductive to the improvement of visible photocatalytic activity.[29,30] The photoresponse range can be expanded by generation of oxygen vacancies that could narrow the band gap by formation of oxygen-vacancy states located within the band gap. Moreover, oxygen defects could also serve as photoinduced charge traps to prevent the electron−hole recombination and as adsorption sites where the charges were transferred to adsorbed species.[29,30]

Very recently, carbon nanodot–carbon nitride nanocomposites have demonstrated impressive performance for efficient photocatalytic water splitting, which is associated with the coupled photocatalysis and chemical catalysis.[31] This work inspires us to prepare environmental catalyst that can utilize thermal and solar energy simultaneously. Recently, $(BiO)_2CO_3$ is found to be an emergent semiconductor photocatalyst.[32-35] However, the pristine $(BiO)_2CO_3$ exhibits low visible light photocatalytic activity and no thermal catalytic activity. It is most appealing to make the $(BiO)_2CO_3$ both visible light active and thermally active for efficient pollutants removal.

Herein, black defective $(BiO)_2CO_3$ catalyst was synthesized by heat treating of pure $(BiO)_2CO_3$ in vacuum. It was found for the first time that this novel catalyst can serve as both active thermal catalyst which could abate pollutant at room temperature and photocatalyst which can efficiently utilize visible light. Thorough investigation indicated that the obtained samples consisted of $(BiO)_2CO_3$ phase, Bi element phase and Bi^{5+}, accompanying with the generation of oxygen defects. Theses active components (Bi^0, Bi^{5+}, oxygen defects) could make the black $(BiO)_2CO_3$ active in the dark and under visible irradiation. In the dark, the black $(BiO)_2CO_3$ microspheres exhibited impressive high catalysis for NO removal at room temperature. Under visible light irradiation, highly efficient activity for NO removal was achieved, which is attributed to the synergy of thermocatalysis and visible light photocatalysis. The detailed mechanisms for the room temperature catalysis and the enhanced catalysis under visible light irradiation were proposed based on in situ DRIFTS, EPR and so on. The present work could provide new insights into the development of new environmental catalysts with bi-functional catalysis behavior for wide potential applications in air purification, hydrogen production or organic synthesis.

2. Experimental section

2.1 Synthesis.

2.1.1 Synthesis of the pure $(BiO)_2CO_3$. All chemicals used in this study were analytical grade (Sigma-Aldrich). The pure $(BiO)_2CO_3$ superstructures were prepared using a modification of the method reported by our previous work[32]. Briefly, 1.60 g of bismuth citrate and 0.46 g of sodium carbonate were mixed with 75 mL of water in a 100 mL autoclave Teflon vessel and stirred for 30 min. The resulting aqueous precursor suspension was then hydrothermally treated at 160 ^oC for 36 h. The precipitates obtained was filtered, washed with water and ethanol for three times and dried at 60 ^oC for 12 h to obtain final $(BiO)_2CO_3$ with no further treatment. The pure $(BiO)_2CO_3$ with white colour was labelled as BOC.

2.1.2 Synthesis of the black defective $(BiO)_2CO_3$. 1.5 g of the prepared $(BiO)_2CO_3$ was put into the vacuum tube, and the pressure was set at 50 mmHg. The black samples, obtained by vacuum heat treating the pure $(BiO)_2CO_3$ with temperature setting at 250, 275 and 300 ^oC for 3 h, were denoted as BOC-250, BOC-275 and BOC-300, respectively. And the samples after catalytic test were labeled as BOC-after, BOC-250-after, BOC-275-after and BOC-300-after, separately.

2.2 Characterization

The crystal phases of the sample were analyzed by X-ray diffraction (XRD) with Cu Kα radiation (model D/max RA, Rigaku Co., Japan). X-ray photoelectron spectroscopy (XPS) with Al Kα X-rays (Thermo ESCALAB 250, USA) was used to investigate the surface properties. Scanning electron microscopy (SEM; model JSM-6490, Japan) was used to characterize the morphology of the obtained products. The morphology and structure of the samples were examined by transmission electron microscopy (TEM; JEM-2010, Japan). The UV-vis diffuse-reflectance spectra were obtained for the dry-pressed disk samples using a Scan UV-vis spectrophotometer (UV-vis DRS: UV-2450, Shimadzu, Japan) equipped with an integrating sphere assembly, using 100% $BaSO_4$ as the reflectance sample. Nitrogen adsorption–desorption isotherms were obtained on a nitrogen adsorption apparatus (ASAP 2020, USA). The electron paramagnetic resonance (EPR) spectra were collected using a Bruker ESP 500 spectrometer at

77 K in the dark and under the light irradiation of 420 nm. Steady and time-resolved fluorescence emission spectra were recorded at room temperature with a fluorescence spectrophotometer (Edinburgh Instruments, FLSP-920).

2.3 DRIFTS study on catalytic NO oxidation.

In situ DRIFTS experiments were carried out by using Bruker Tensor 27 FT-IR spectrometers. Catalysts were pretreated at room temperature under He (30 mL/min) for 60 min to remove adsorbed impurities. After the background spectrum was recorded with the flowing of He and was subtracted, the samples were then exposed to 300 ppm of NO with 20% O_2. DRIFTS spectra of samples were recorded at room temperature by accumulating 32 scans with a resolution of 4 cm^{-1} at a given interval.

2.4 Thermal catalytic and visible light photocatalytic performance for NOx removal.

The performance was measured by removal of NOx at ppb levels in a continuous flow reactor at ambient temperature.[20] The volume of the rectangular reactor, made of polymeric glass and covered with Saint-Glass, was 4.5 L (30 cm × 15 cm × 10 cm). The NO gas was acquired from a compressed gas cylinder at a concentration of 100 ppm of NO (N_2 balance). The initial concentration of NO was diluted to about 600 ppb by the air stream supplied compressed air. The desired relative humidity (RH) level of the NO flow was controlled at 50% by passing the zero air streams through a humidification chamber. The gas streams were premixed completely by a gas blender, and the flow rates of the air stream and NO were controlled at 2.4 L/min and 15 mL/min by a mass flow controller. The catalyst (1.0 g) was coated on two dishes with a diameter of 12.0 cm. For the room temperature performance test, the rectangular reactor was surrounded by tinfoil, and no light or extra heat energy was provided. For the catalytic activity test under visible light, a 150 W commercial tungsten halogen lamp was vertically placed outside the reactor, and a UV cut off filter (420 nm) was adopted to remove UV light in the light beam. The concentration of NOx was continuously measured by a chemiluminescence NOx analyzer (Thermal, model 42i-TL), which monitors NO, NO_2, and NOx (NOx represents NO + NO_2) with a sampling rate of 1.0 L/min. The removal ratio (η) of NOx was calculated as $\eta(\%) = (1-C/C_0) \times 100\%$, where C and C_0 are concentrations of NOx in the outlet steam and the feeding stream, respectively.

3. Results and discussion

3.1 Room temperature catalysis and visible light photocatalysis for NO removal.

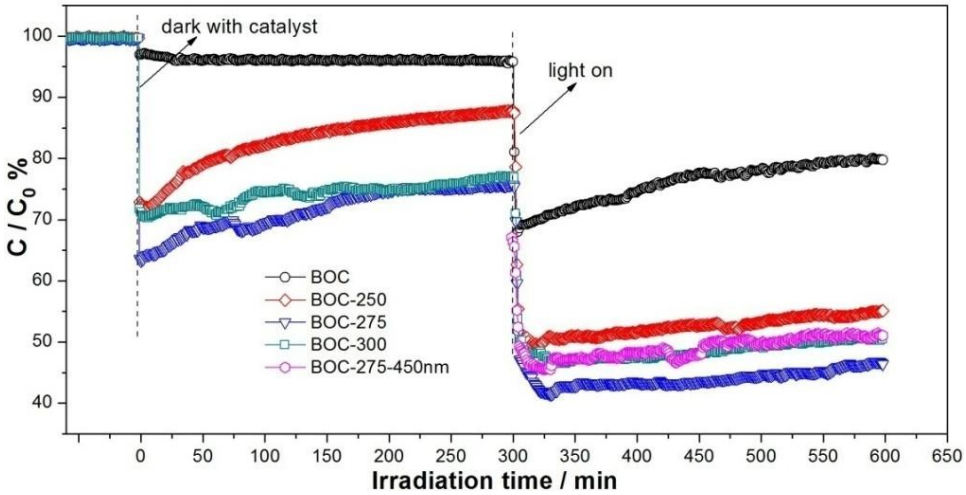

Fig. 1 Comparison of the catalytic removal of NO in the dark and under the visible light irradiation over the as-prepared samples.

The prepared BOC and the vacuum treated $(BiO)_2CO_3$ samples were applied for NO removal in the dark and with visible light irradiation as shown in Fig. 1. As we know, the self-removal of NO can be ignorable at room temperature or under visible light irradiation.[32] In the presence of BOC, almost no activity could be observed when the system is kept in the dark. When the light is turned on, BOC displays a low activity with a NO removal ratio of 19.0%, and the activity stems from the scattering and reflection effects as the bandgap of BOC is too large to be excited by visible light.[33]

However, to our surprise, after vacuum heat treatment, the obtained black samples show room temperature catalytic activity in the dark. BOC-250, BOC-275 and BOC-300 exhibit NO removal ratio of 28.1, 30.0 and 37.0%, respectively. Later, the NO removal ratio gradually decreases to 12.3, 24.2 and 23.1% probably due to the reduced active sites. Once the visible light is provided, the black samples display highly enhanced activity. BOC-250 presents a high NO removal percentage of 50.1%. For BOC-275, an admirable removal ratio of 59.6% is attained.

Further increasing the heat treatment temperature would result in a decreased activity of 53.6% for BOC-300. Note that the catalytic performance under visible light irradiation is relatively stable, and the removal ratio is higher than that of the bare thermocatalysis. This result implies that the contribution ratio of photocatalysis is higher than that of thermocatalysis. In addition, when the light with a long-pass cutoff filter allowing $\lambda > 450$ nm is adopted to irradiate BOC-275 (denoted as BOC-275-450nm), a significant activity is observed as well. In a word, the vacuum heat treated samples exhibit extraordinarily high catalytic performance for NO removal compared with the white BOC no matter whether it is in the dark or under visible light. This is the first time that room temperature thermal catalysis and visible light photocatalysis can be integrated within black $(BiO)_2CO_3$ catalyst, which could represent a new and appealing technology for NO treatment. Next, extensive investigations were carried out on the obtained samples to reveal the driving force for the unexpected performance of black $(BiO)_2CO_3$ in NO removal.

3.2 Phase and chemical composition.

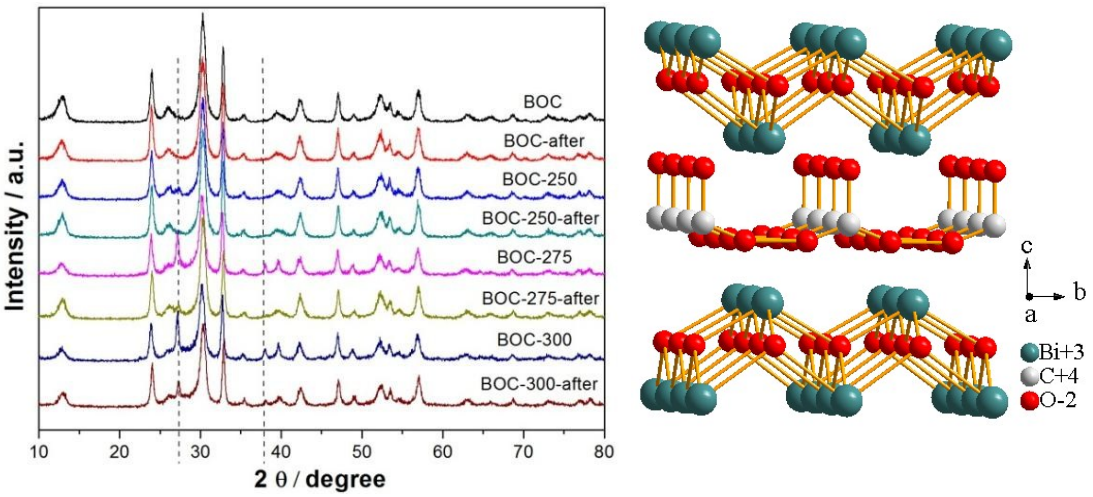

Fig. 2 XRD patterns of the BOC and the black samples before and after catalytic test (left) and crystal structure of $(BiO)_2CO_3$ (right).

Fig. 2 shows the typical XRD pattern of the BOC and vacuum-treated $(BiO)_2CO_3$ at 250, 275 and 300 °C. All peaks of BOC can be nicely indexed to the pure $(BiO)_2CO_3$ (JCPDS-ICDD card no. 25-1464). For the vacuum heat treated samples, the major phase identified is $(BiO)_2CO_3$. Notably, a small amount of Bi element (JCPDS card no. 05-0519) with the diffraction peaks at 27.2 and 37.9 °corresponding to the (012) and (104) diffraction planes can be observed. Bi element originates from the reduction of Bi^{3+}, which may induce the generation of oxygen defects in the $(Bi_2O_2)^{2+}$ layers according to the crystal structure simultaneously. Also, with the increase in vacuum treatment temperature, the diffraction peaks of Bi are intensified gradually.

Nevertheless, the peaks intensity corresponding to Bi element decreases after the catalytic performance test, which indicates the reduction of the Bi^0 sites. This is consistent with the gradually decreased activity as the reaction time increases. The gradual deactivation of catalyst has been observed for many other typical catalysts,[36,37] which can be solved by activation and regeneration.

To verify the surface compositions and chemical states of the as-obtained samples further, X-ray photoelectron spectroscopy (XPS) was employed as shown in Fig. S1 (ESI†). The characteristic peaks for Bi^{3+} in $(BiO)_2CO_3$ at the binding energy of ~159.15 and 164.45 eV are indicative of Bi $4f_{7/2}$ and Bi $4f_{5/2}$, respectively (Fig. S1a). For the black samples, except for the peaks of Bi^{3+}, additional peaks belonging to Bi^0 (about 158 and 163.4 eV) and Bi^{5+} (ca. 160.6 and 165.9 eV) can be detected, and the peak intensity of Bi^0 and Bi^{5+} increases with the increased vacuum treatment temperature (Fig. S1b, S1c and S1d).[38] Based on this finding, we can conclude that some Bi^{3+} disproportionated to Bi^0 and Bi^{5+} under vacuum heat treatment. However, the peak intensity of Bi^0 and Bi^{5+} for BOC-300-after decreases (Fig. S2), in agreement with the XRD results.

3.3 Morphological structure.

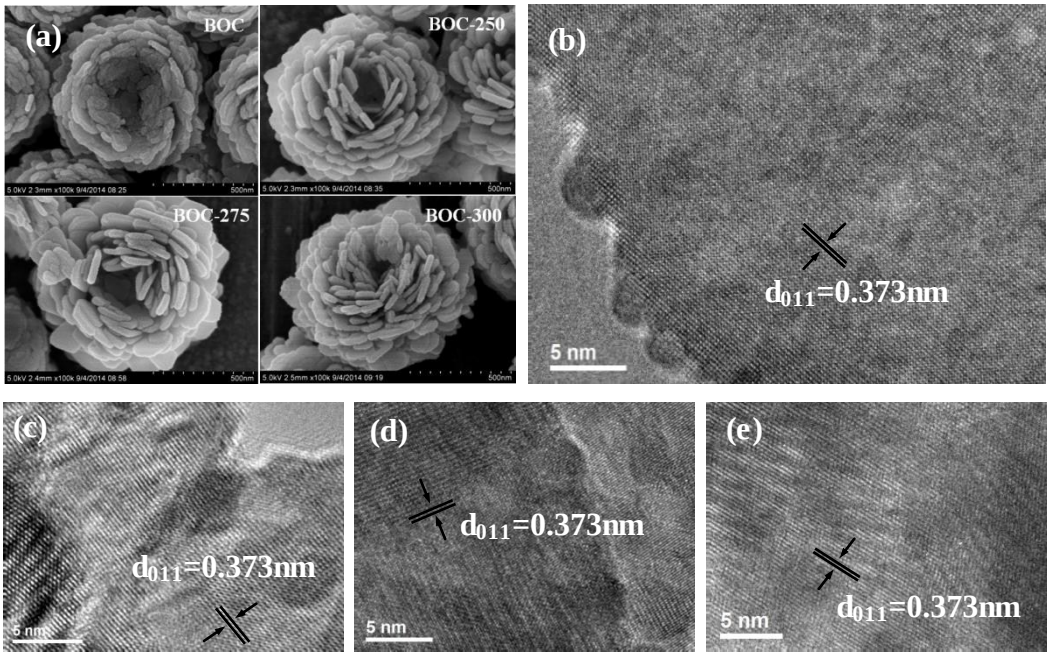

Fig. 3 SEM images of the as-prepared samples (a) and HRTEM images of BOC (b), BOC-250 (c), BOC-275 (d) and BOC-300 (e).

The morphology of the as-prepared samples was then determined from SEM and TEM. The SEM images demonstrate that the four samples possess similar flower-like hierarchical structure (Fig. S3), suggesting that the vacuum heat treatment does not break the morphology. A closer observation indicates the microspheres assembled from numerous nanosheets (Fig. 3a). The assembly of the nanosheets may produce abundant hierarchical pores on nanoscale. These nanosheets are densely packed and a hollow structure in the center can be observed, which are further evidenced by TEM image in Fig. S4. A well-defined crystalline lattice can be identified with a d-spacing of 0.373 nm corresponding to (011) plane of $(BiO)_2CO_3$ for the four samples (Fig. 3b, 3c, 3d and 3e). In addition, the morphologies of BOC-after, BOC-250-after, BOC-275-after and BOC-300-after are the same with the fresh samples (Fig. S5). Also, the major (011) crystalline planes with 0.373 nm distance of $(BiO)_2CO_3$ are dominantly observed for BOC-300-after (Fig. S5h). These results confirm the stability of the morphology after exposed to light and pollutants.

The specific surface area and porosity property of the four samples were analyzed by N_2 adsorption-desorption measurement. Typical IV isotherms with H3-type hysteresis loops are found, demonstrating the existence of mesoporous structure (Fig. S6a).[39] The mesoporous nature is further corroborated by the result where a wide pore size distribution of between 10-100 nm is observed (Fig. S6b), which also indicates the presence of macropores. The mesopores are created by aggregation of the $(BiO)_2CO_3$ nanosheets as observed in SEM (Fig. 3). These pores not only benefit the absorption of light via scattering and reflection effects, but also favor the diffusion of reactants and products.[40] Additionally, the specific surface area of BOC, BOC-250, BOC-275 and BOC-300 is 29.1, 27.8, 23.7 and 15.3 m^2/g, respectively.

3.4 The nature of defects.

To confirm the nature and existence of oxygen vacancies, electron paramagnetic resonance (EPR) of the as-obtained samples was performed at 77 K (Fig. 4). No matter whether it is in the dark or under visible light illumination, nearly no signs can be found for pure BOC. While for the samples with vacuum heat treatment, symmetric peaks centered at g = 2.001 are detected, which can be attributed to paramagnetic oxygen vacancies about the surface.[41,30] Under visible light illumination, the signal intensity remains the same as that in the dark. It can be concluded that the visible light does not affect the oxygen vacancy. As presented in the introduction part, the oxygen vacancy introduced in the crystal structure could contribute to the enhancement of thermocatalysis and photocatalysis. According to the crystal structure (Fig. 1), in conjunction with the analysis of XRD and XPS, the oxygen defects are considered to be existed in the $(Bi_2O_2)^{2+}$ layers.

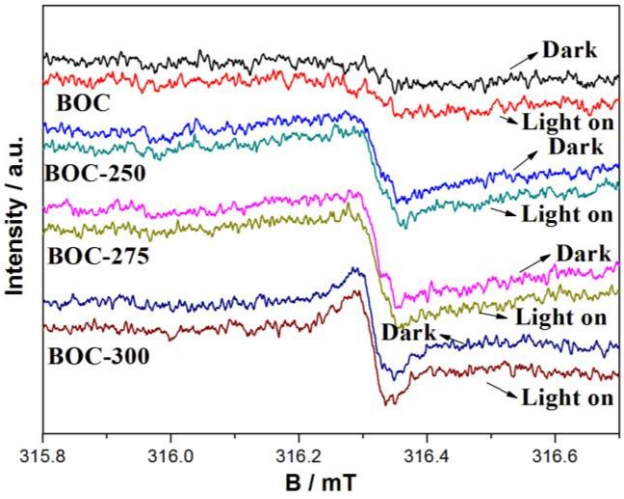

Fig. 4 Solid state EPR spectra recorded at 77K for the as-prepared samples in the dark and under visible light illumination.

3.5 In situ DRIFT investigation.

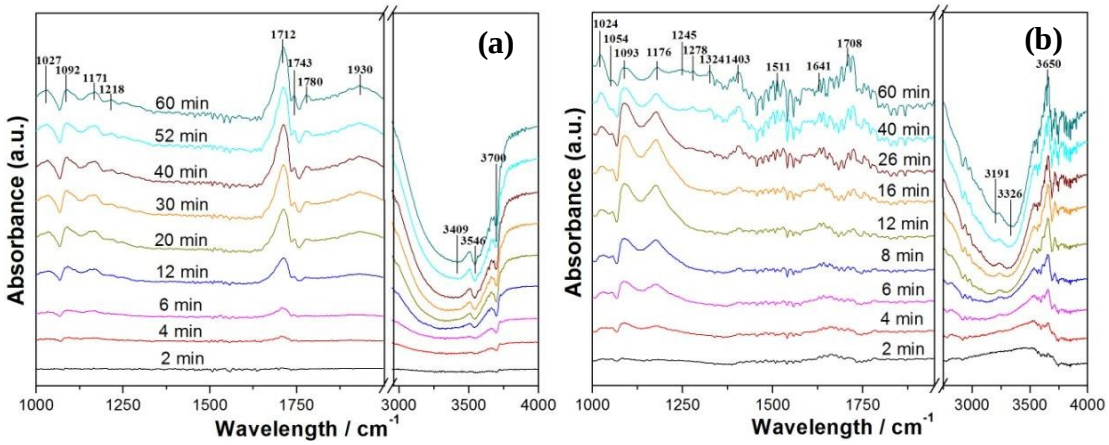

Fig. 5 In situ DRIFTS spectra of (a) BOC and (b) BOC-300 treated in flowing 300 ppm NO + 20% O_2 at room temperature for 60 min.

In order to explore the origin of the room temperature catalytic activity of black defective $(BiO)_2CO_3$ microspheres, in situ DRIFTS spectra of the NO + O_2 co-action on BOC-300 at room temperature were recorded, together with BOC as a comparison as shown in Fig. 5. As displayed in Fig. 5a, when NO + O_2 is adsorbed onto BOC for 20 min, a series of bands ascribed to NO adspecies appear. The bands at 1027 and 1218 cm^{-1} are assigned to the bidentate nitrates and nitrites,[42,43] whereas the bands at 1092 and 1171 cm^{-1} are attributed to $N_2O_2^{2-}$ and NO^- species, respectively.[44] In addition, NO could interact with surface metal centers, giving rise to surface nitrosyl species.[45,46] Thus, the bands at 1712, 1743, 1780 and 1930 cm^{-1} are supposed to be ascribed to the $[Bi(NO)_n]^{3+}$ ($1<n<5$). In the OH stretching region, negative absorption bands at 3409, 3546 and 3700 cm^{-1} can be indexed to isolated surface OH^- groups. The negative bands could be associated with the consumption of the OH groups.[47] By increasing the exposure time, no new bands appear except that the intensity of the bands grows step by step.

As depicted in Fig. 5b, when BOC-300 is exposed to NO+O_2 for 16 min, except the absorption bands at 1024, 1093, 1176 and 1708 cm^{-1} can be observed, some new bands related to nitrate or nitrite species develop. The bands at 1054 cm^{-1} are attributed to the bridging nitrates. The bands at 1403 and 1511 cm^{-1} belong to NO_2^- and NO_3^-, respectively.[48,49] In addition, the bands at ~1641 cm^{-1} corresponding to NO_2 can be detected.[50] By increasing the exposure time, there is a decrease in the intensity of these bands at 1024, 1054, 1093 and 1176 cm^{-1}. Meanwhile, some bands are newly formed at 1245, 1278 and 1324 cm^{-1} assignable to the nitrate and nitrites, respectively.[44] This observation indicates the NO adspecies with lower stability are desorbed on the surface and then transformed into stable nitrates or nitrites. In the OH stretching region, two broad negative bands centered at 3191 and 3326 cm^{-1} are also observed. Moreover, a weak positive band observed at 3650 cm^{-1} reveals the presence of H-bonded hydroxyls.[51]

The DRIFTS spectroscopic results clearly demonstrate the different behaviors of NO + O_2 over the two catalysts.

NO molecules mainly exist in the form of NO adspecies on BOC. However, except for the NO adspecies, NO molecules could easily transform into stable nitrates or nitrites on BOC-300. Li et al. suggested that fractional charged Au species could be the active sites for formaldehyde oxidation over a gold/iron oxide catalyst.[52] Here, the Bi species are considered to be active sites. In addition, the oxygen defects with single electron in BOC-300 can donate electrons to the surrounding molecular. Combined with the result analyzed by XRD, XPS and EPR, we propose a room temperature catalysis mechanism for NO removal involved with the Bi^{5+}, Bi^0 and oxygen vacancy. When BOC-300 is exposed to oxygen and nitrogen monoxide, it is thought that oxygen molecules are adsorbed and become negatively charged via obtaining electrons from the oxygen defects (reaction (1)). NO molecules are adsorbed on the active species such as Bi^{5+} and Bi^0 sites, which then react with O_2^- to produce NO_3^- (reaction (2)). Also, NO can react with O_2 to produce NO_2 at the active species sites (reaction (5)). Meantime, NO and NO_2 can obtain electrons from the oxygen defects to create NO^- and NO_2^- (reaction (3) and (6)) as well. Then, the NO and NO^- can obtain an electron form oxygen defects to produce $N_2O_2^{2-}$ (reaction (4)). While for BOC, few $N_2O_2^{2-}$ and NO^- species can be detected mainly due to the existence of some intrinsic defects in $(BiO)_2CO_3$.

$$V_O \bullet + O_2 \rightarrow O_2^- \quad (1)$$

$$O_2^- + NO \rightarrow NO_3^- \quad (2)$$

$$NO + V_O \bullet \rightarrow NO^- \quad (3)$$

$$NO + NO^- + V_O \bullet \rightarrow N_2O_2^{2-} \quad (4)$$

$$2NO + O_2 \rightarrow 2NO_2 \quad (5)$$

$$NO_2 + V_O \bullet \rightarrow NO_2^- \quad (6)$$

3.6 Light absorption, carriers transfer and catalysis mechanisms.

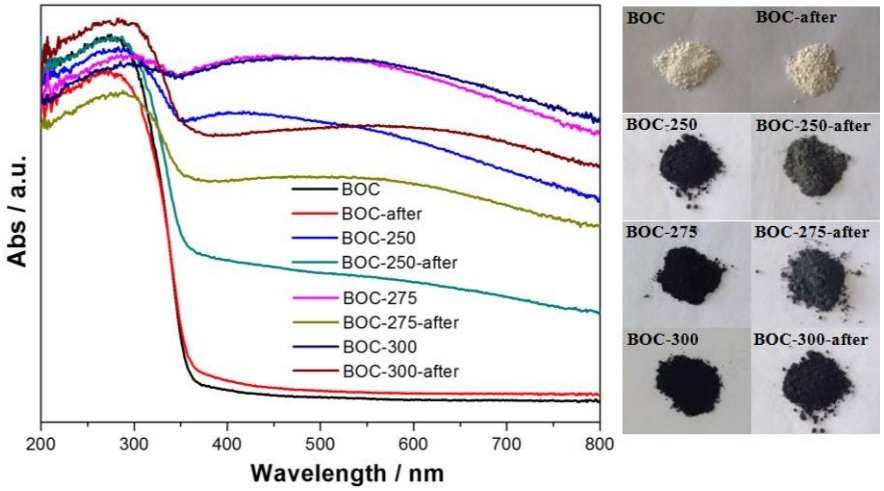

Fig. 6 UV-vis DRS and the corresponding color of the as-prepared samples before and after catalytic test.

In subsequent studies, the photoabsorption property of these samples were studied as shown in Fig. 6, BOC shows the photoabsorption in UV light region with the wavelength shorter than 360 nm and almost nearly no absorption in the visible light region. In contrast, the vacuum-treated samples show full absorption in the UV and visible region, consistent with the color change from white to black. This may benefit from the oxygen defects introduced in the crystal structure by vacuum heat treatment, which can narrow the band gap and then extend the light response from UV to visible light. Schmuki et.al reported that hydrogenated anatase with specific defect centers showed strong visible light absorption and photocatalytic dihydrogen evolution.[53] Chen and co-workers also observed that TiO_2 nanocrystals with oxygen vacancy and Ti^{3+} defects showed long-wavelength optical absorption and high photocatalytic activities.[29] Besides, Bi elements, possessing plasmonic effect, can contribute to the improved visible light absorption because of its plasmonic resonance absorption. However, the samples after catalytic test present decrease in light absorption. Coincidentally, the black color becomes shallow.

To investigate the photophysical property of photoexcited charge carriers, the ns-level time-resolved fluorescence decay spectra of BOC and BOC-275 were recorded as shown in Fig. 7a and 7b. The radiative lifetime with different percentages can be determined by fitting the decay spectra, as summarized in Table 1. The short lifetime τ_1 of BOC is 0.168 ns. After vacuum treatment, the short lifetime of BOC-275 is increased up to 0.350 ns. On the other hand, the long lifetime τ_2 of charge carriers is increased from 0.503 ns for BOC to 1.344 ns for BOC-275 (Table 1). These results imply that the radiative lifetime of all charge carriers are increased for samples after vacuum treatment. The oxygen defects which can serve as charge traps to prevent the electron−hole recombination to prolong lifetime of charge carriers.[30] Furthermore, the Bi element with plasmonic effect, similar to noble metals, could create electric field to enhance the surface electron excitation and interfacial electron transfer.[54] The prolonged lifetime of charge carriers could increase its probability of being captured by reactive

substrates to initiate the photocatalytic reactions.

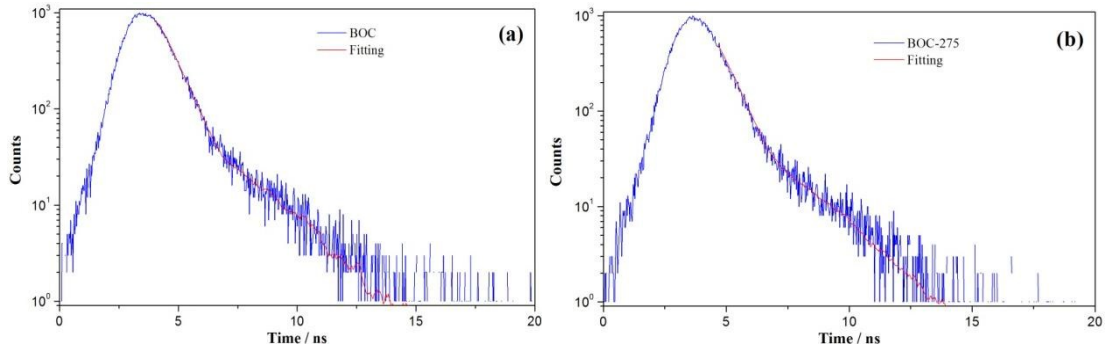

Fig. 7 The ns-level time-resolved fluorescence spectra monitored at 380 nm under 375 nm excitation at room temperature for BOC and BOC-275.

Table 1. The kinetics of emission decay parameters of the BOC and BOC-275 samples (χ denotes the fitting degree of the fitted curve with the experimental results).

Samples	Component	Life time (ns)	Relative Percentage (%)	χ^2
BOC	τ_1	0.168	66.1	1.013
	τ_2	0.503	33.9	
BOC-275	τ_1	0.350	96.0	1.087
	τ_2	1.344	4.0	

Based on the above analysis, we can provide the reasons accounting for the phenomena that the black samples own catalytic activity in the dark and enhanced activity under visible light. In the dark, the active sites (Bi^0, Bi^{5+}) activate the NO molecules, while the oxygen defects can directly activate NO or activate the adsorbed O_2 to produce active species. Then the active NO molecules react with the active species and generate nitrogen dioxide, nitrite and nitrate. It is reported that light energy can be partially transformed into thermal energy and then benefit the thermocatalytic reaction.[55] Thus, under the irradiation of visible light, partial light energy transforms to thermal energy, promoting the surface thermocatalytic reaction over the as-prepared black samples.

In addition, introducing oxygen detects in the crystal structure by vacuum heat treatment can narrow the bandgap of $(BiO)_2CO_3$ and subsequently extend the light response to visible light region. Namely, the electrons in the localized electronic states can be excited by visible light to the conduction band. As investigated by our previous report, the photogenerated holes and OH are found to be the main active species for $(BiO)_2CO_3$ to remove NOx. Here, similarly, the holes in localized states after photoexcitation can be directly involved in the photocatalytic reaction or generate OH to induce chemical reaction.[33] Also, the Bi element with plasmonic effect assists in the separation of photoinduced electrons and holes.[54] Nevertheless, the decrease in the catalytic performance for samples fabricated at high treatment temperature is mainly attributed to the fact that excessive oxygen defects could act as recombination centers.[30] Generally, the dark activity is dominated by the thermocatalysis and the enhanced visible catalytic performance results from the synergy of thermocatalysis and photocatalysis. The mechanisms of the catalysis in the dark and under visible light are illustrated in the Scheme 1.

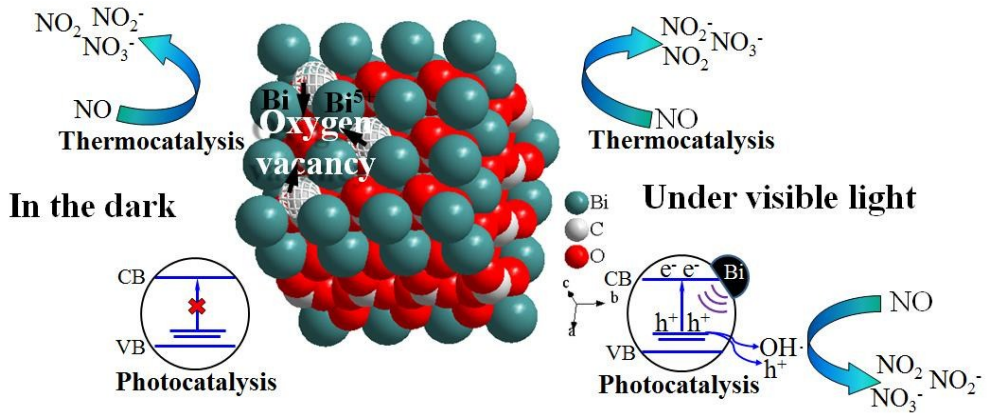

Scheme 1. The illustration of the mechanism about catalysis in the dark and under visible light for NOx removal.

3.7 Activation and regeneration of the used catalyst.

The prepared catalysts contain $(BiO)_2CO_3$, Bi^0, Bi^{5+} and oxygen defects. These compositions enabls the catalysts to absorb the light in the whole range and then the catalysts exhibit black color. Also, these active compositions make the catalysts active both in the dark and under visible light irradiation. However, these active compositions would be deactived during photocatalysis reaction. As can be seen, with the NO removal reaction continuing, the active compositions decrease and then lead to lowered activity. Even though the prepared catalysts are exposed to air without participating in the removal of NO, the catalysts will be deactivated and the color will become shallow as a result of the reduction of active compositions. Namely, the prepared samples show decreased activity gradually due to the decrease of the active sites. After exposed to the air for half a year, these active sites are reduced, and the color of the samples becomes off-white (Fig. S7a). The deactivation is normal for most of the catalysts. It is most important to develop a facile method to activate the used catalyst. Then, we applied the deactivated samples for a secondary vacuum heat treatment to regenerate the catalyst. Similarly, the color of the samples become black (Fig. S7b). The XRD and SEM of the regenated samples are the same with those of the first prepared catalyst (Fig. S7c and S7d). Also, we test the performance of the regenerated sample for NO removal. As shown in Fig. S7e, the sample exhibits almost the same efficient activity as the fresh sample. This fact implies that the deactivated catalyst can be easily activated with a secondary vacuum heat treatment for recycled application.

4. Conclusion

In summary, a black defective $(BiO)_2CO_3$ catalyst has been fabricated and its high NO removal performance at room temperature in dark and under visible light irradiation was first demonstrated. The catalyst contained $(BiO)_2CO_3$ phase, Bi element phase, Bi^{5+} and oxygen defects. The active sites (Bi^0, Bi^{5+}, oxygen defects) tended to absorb the NO molecules and then weakened their bonds, while the oxygen defects can directly activate the adsorbed O_2 to generate the active species. Then the adsorbed NO molecules reacted with the active species to create nitrogen dioxide, nitrite and nitrate in the dark. Once the visible light was applied, thermal energy originating from the transformation of partial light energy could accelerate the surface thermocatalytic reaction. The narrowed band gap of $(BiO)_2CO_3$ caused by the oxygen defects, along with the plasmonic effect of Bi element could make the black $(BiO)_2CO_3$ highly visible light active. Consequently, the efficient dark catalytic activity benefited from the thermocatalysis and the enhanced visible catalytic photocatalytic performance was ascribed to the synergy of thermocatalysis and photocatalysis. This work integrates the concepts of thermocatalysis and photocatalysis into one typical catalyst for admirable catalytic NO removal, and could provide a new perspective for environmental catalysts development and application.

Acknowledgments

This research is financially supported by the National Natural Science Foundation of China (51478070, 51108487), and the Innovation Project for Postgraduates from Chongqing Education Commission (CYS14172).

Notes and references

(1) L. S. Brickus, J. N. Cardoso and F. R. de Aquino Neto, *Environ. Sci. Technol*., 1998, **32**, 3485.
(2) Y. Zhao, L. Duan, T. Larssen, L. H. Hu and J. M. Hao, *Environ. Sci. Technol*., 2007, **41**, 1815.
(3) K. Skalska, J. S. Miller and S. Ledakowicz, *Sci. Total Environ*., 2010, **408**, 3976.
(4) H. Y. Huang and R. T. Yang, *Langmuir*, 2001, **17**, 4997.
(5) B. H. Lu, Y. Jiang, L. L. Cai, N. Liu, S. H. Zhang and W. Li, *Bioresour. Technol*., 2011, **102**, 7707.
(6) C. Liu, L. Chen, J. Li, L. Ma, H. Arandiyan, Y. Du, J. Xu and J. Hao, *Environ. Sci. Technol*., 2012, **46**, 6182.
(7) M. Kaneeda, H. Iizuka, T. Hiratsuka, N. Shinotsuka and M. Arai, *Appl. Catal. B: Environ*., 2009, **90**, 564.
(8) G. Li, D. Zhang, J. C. Yu and M. K. H. Leung, *Environ. Sci. Technol*., 2010, **44**, 4276.
(9) N. An, Q. Yu, G. Liu, S. Li, M. Jia and W. Zhang, *J. Hazard. Mater*., 2011, **186**, 1392.
(10) H. F. Li, N. Zhang, P. Chen, M. F. Luo and J. Q. Lu, *Appl. Catal. B: Environ*., 2011, **110**, 279.
(11) Z. Zheng, J. Teo, X. Chen, H. Liu, Y. Yuan, E. R. Waclawik, Z. Zhong and H. Zhu, *Chem. Eur. J*., 2010, **16**, 1202.
(12) X. Tang, Y. Li, X. Huang, Y. Xu, H. Zhu, J. Wang and W. Shen, *Appl. Catal. B: Environ*., 2006, **62**, 265.
(13) M. A. Sidheswaran, H. Destaillats, D. P. Sullivan, J. Larsen and W. J. Fisk, *Appl. Catal. B: Environ.*, 2011, **107**, 34.
(14) E. Wahlstrom, E. K. Vestergaard, R. Schaub, A. Ronnau, M. Vestergaard, E. Laegsgaard, I. Stensgaard and F. Besenbacher, *Science*, 2004, **303**, 511.
(15) J. Guzman, S. Carrettin and A. Corma, *J. Am. Chem. Soc*., 2005, **127**, 3286.
(16) J. Guzman, S. Carrettin, J. C. Fierro-Gonzalez, Y. Hao, B. C. Gates and A. Corma, *Angew. Chem. Int. Ed*.,

2005, **44**, 4778.
(17) M. Setvín, U. Aschauer, P. Scheiber, Y. F. Li, W. Hou, M. Schmid, A. Selloni and U. Diebold, *Science*, 2013, **341**, 988.
(18) L. Zeng, W. Song, M. Li, D. Zeng and C. Xie, *Appl. Catal. B: Environ.*, 2014, **147**, 490.
(19) Z. Ai, W. Ho, S. Lee and L. Zhang, *Environ. Sci. Technol.*, 2009, **43**, 4143.
(20) F. Dong, Z. Wang, Y. Li, W. K. Ho and S. C. Lee, *Environ. Sci. Technol.*, 2014, **48**, 10345.
(21) W. J. Jiang, J. A. Joens, D. D. Dionysiou**,** K. E. O'Shea, *J. Photochem. Photobiol. A: Chem.*, 2013, **262**, 7.
(22) F. Dong, T. Xiong, Y. Sun, Z. Zhao, Y. Zhou, X. Feng and Z. Wu, *Chem. Commun*., 2014, **50**, 10386.
(23) A. Fujishima, X. Zhang and D. A. Tryk, *Surf. Sci. Rep.* 2008, **63**, 515.
(24) T. Ochiai and A. Fujishima, *J. Photochem. Photobiol. C*, 2012, **13**, 247.
(25) R. Asahi, T. Morikawa, H. Irie and T. Ohwaki, *Chem. Rev*., 2014, **114**, 9824.
(26) T. Xiong, H. W. Huang, Y. J. Sun, F. Dong, *J. Mater. Chem. A*, 2015, **3**, 6118-6127.
(27) Y. He, L. Zhang, B.-T. Teng and M. Fan, *Environ. Sci. Technol.*, 2015, **49**, 649.
(28) H. Wang, L. Zhang, Z. Chen, J. Hu, S. Li, Z. Wang, J. Liu and X. Wang, *Chem. Soc. Rev*., 2014, **43**, 5234.
(29) T. Xia, Y. Zhang, J. Murowchick and X. Chen, *Catal. Today*, 2014, **225**, 2.
(30) Y. Lv, Y. Zhu and Y. Zhu, *J. Phys. Chem. C*, 2013, **117**, 18520.
(31) J. Liu, Y. Liu, N. Liu, Y. Han, X. Zhang, H. Huang, Y. Lifshitz, S.-T. Lee, J. Zhong and Z. Kang, *Science*, 2015, **347**, 970.
(32) F. Dong, A. M. Zheng, Y. J. Sun, M. Fu, B. Q. Jiang, W. K. Ho, S. C. Lee and Z. B. Wu, *CrystEngComm*, 2012, **14**, 3534.
(33) T. Xiong, F. Dong and Z. Wu, *RSC Adv*., 2014, **4**, 56307.
(34) F. Qin, G. Li, R. Wang, J. Wu, H. Sun and R. Chen, *Chem. Eur. J*., 2012, **18**, 16491.
(35) J. Tang, H. Zhao, G. Li, Z. Lu, S. Xiao and R. Chen, *Ind. Eng. Chem. Res*., 2013, **52**, 12604.
(36) Y. Hou, A. B. Laursen, J. Zhang, G. Zhang, Y. Zhu, X. Wang, S. Dahl and I. Chorkendorff, *Angew. Chem. Int. Ed.*, 2013, **52**, 1.
(37) H. Gao, S. Yan, J. Wang, Y. A. Huang, P. Wang, Z. Li and Z. Zou, *Phys. Chem. Chem. Phys*., 2013, **15**, 18077.
(38) Y. Fujimoto, Mikhail Grishin (Ed.), InTech, 2010.
(39) K. S. W. Sing, D. H. Everett, R. A. W. Haul, L. Moscou, R. A. Pierotti, J. Rouquerol and T. Siemieniewska, *Pure Appl. Chem*., 1985, **57**, 603.
(40) C. M. A. Parlett, K. Wilson and A. F. Lee, *Chem. Soc. Rev*., 2013, **42**, 3876.
(41) Z. Wang, W. Ma, C. Chen, H. Ji and J. Zhao, *Chem. Eng. J.*, 2011, **170**, 353.
(42) B. Azambre, L. Zenboury, A. Koch and J. V. Weber, *J. Phys. Chem. C*, 2009, **113**, 13287.
(43) B. Azambre, I. Atribak, A. Bueno-López and A. García-García, *J. Phys. Chem. C*, 2010, **114**, 13300.
(44) M. Chen, Z. Wang, D. Han, F. Gu and G. Guo, *J. Phys. Chem. C*, 2011, **115**, 12763.
(45) G. Berlier, C. Lamberti, M. Rivallanw and G. Mul, *Phys. Chem. Chem. Phys*., 2010, **12**, 358.
(46) L. Wang, G. Wang, H. Qu, Z. H. Li and M. Zhou, *Phys. Chem. Chem. Phys*., 2014, **16**, 10788.
(47) N. Apostolescu, T. Schroder and S. Kureti, *Appl. Catal. B: Environ.*, 2004, **51**, 43.
(48) J. C. S. Wu and Y. T. Cheng, *J. Catal.*, 2006, **237**, 393.
(49) G. S. Qi, R. T. Yang and R. Chang, *Appl. Catal. B: Environ.*, 2004, **51**, 93.
(50) G. Ramis, G. Busca, V. Lorenzelli and P. Forzatti, *Appl. Catal.*, 1990, **64**, 243.
(51) M. J. Kantcheva, *J. Catal.*, 2001, **204**, 479.
(52) C. Y. Li, Y. N. Shen, M. L. Jia, S. Sheng, M. O. Adebajo and H. Zhu, *Catal. Commun*. 2008, **9**, 355.
(53) N. Liu, C. Schneider, D. Freitag, U. Venkatesan, V. R. R. Marthala, M. Hartmann, B. Winter, E. Spiecker, A. Osvet, E. M. Zolnhofer, K. Meyer, T. Nakajima, X. Zhou and P. Schmuki, *Angew. Chem. Int. Ed*., 2014, **53**, 1.
(54) F. Dong, Q. Li, Y. Sun and W.-K. Ho, *ACS Catal*., 2014, **4**, 4341.
(55) Y. Ma, Y. Li, M. Mao, J. Hou, M. Zeng and X. Zhao, *J. Mater. Chem. A*, 2015, **3**, 5509.

Graphical Abstract